AGU PUBLICATIONS

Geophysical Research Letters

RESEARCH LETTER
10.1002/2015GL063693

Key Points:
- Lab and field OA elemental composition follow a line in Van Krevelen space
- Mixing and aging largely explain ambient data but gaps exist
- Processing that produce OA with both high O:C and high H:C are needed

Supporting Information:
- Text S1, Figures S1–S3, and Tables S1–S4

Correspondence to:
Q. Chen,
qichenpku@pku.edu.cn

Citation:
Chen, Q., et al. (2015), Elemental composition of organic aerosol: The gap between ambient and laboratory measurements, *Geophys. Res. Lett.*, *42*, 4182–4189, doi:10.1002/2015GL063693.

Received 3 MAR 2015
Accepted 10 APR 2015
Accepted article online 15 APR 2015
Published online 22 MAY 2015

Elemental composition of organic aerosol: The gap between ambient and laboratory measurements

Qi Chen[1,2], Colette L. Heald[1], Jose L. Jimenez[3], Manjula R. Canagaratna[4], Qi Zhang[5], Ling-Yan He[6], Xiao-Feng Huang[6], Pedro Campuzano-Jost[3], Brett B. Palm[3], Laurent Poulain[7], Mikinori Kuwata[8,9], Scot T. Martin[8], Jonathan P. D. Abbatt[10], Alex K.Y. Lee[10], and John Liggio[11]

[1]Department of Civil and Environmental Engineering, Massachusetts Institute of Technology, Cambridge, Massachusetts, USA, [2]Now at State Key Joint Laboratory of Environmental Simulation and Pollution Control, College of Environmental Sciences and Engineering, Peking University, Beijing, China, [3]CIRES and Department of Chemistry and Biochemistry, University of Colorado Boulder, Boulder, Colorado, USA, [4]Aerodyne Research, Inc., Billerica, Massachusetts, USA, [5]Department of Environmental Toxicology, University of California, Davis, California, USA, [6]Key Laboratory for Urban Habitat Environmental Science and Technology, School of Environment and Energy, Peking University Shenzhen Graduate School, Shenzhen, China, [7]Leibniz Institute for Tropospheric Research, Leipzig, Germany, [8]School of Engineering and Applied Sciences, NHarvard University, Cambridge, Massachusetts, USA, [9]Now at Earth Observatory of Singapore, Nanyang Technological University, Singapore, [10]Department of Chemistry, University of Toronto, Toronto, Ontario, Canada, [11]Air Quality Research Division, Environment Canada, Toronto, Ontario, Canada

Abstract A large data set including surface, aircraft, and laboratory observations of the atomic oxygen-to-carbon (O:C) and hydrogen-to-carbon (H:C) ratios of organic aerosol (OA) is synthesized and corrected using a recently reported method. The whole data set indicates a wide range of OA oxidation and a trajectory in the Van Krevelen diagram, characterized by a slope of −0.6, with variation across campaigns. We show that laboratory OA including both source and aged types explains some of the key differences in OA observed across different environments. However, the laboratory data typically fall below the mean line defined by ambient observations, and little laboratory data extend to the highest O:C ratios commonly observed in remote conditions. OA having both high O:C and high H:C are required to bridge the gaps. Aqueous-phase oxidation may produce such OA, but experiments under realistic ambient conditions are needed to constrain the relative importance of this pathway.

1. Introduction

Organic aerosol (OA) is an important, sometimes dominant, component of submicron particle mass in the troposphere [*Zhang et al.*, 2007]. OA particles consist of a large number of individual compounds. The average elemental composition is one approach to simply describe OA chemistry [*Kroll et al.*, 2011]. The O:C and H:C ratios of OA are highly variable, characterizing both the source profiles and the atmospheric evolution of OA [*Heald et al.*, 2010; *Ng et al.*, 2011]. These ratios may also dictate other properties of OA such as hygroscopicity and particle density, both important for evaluating particle dynamics and the climate impacts of OA [*Jimenez et al.*, 2009; *Kuwata et al.*, 2012]. The elemental ratios of OA have been measured in the laboratory and ambient environment using modern mass spectrometry and spectroscopy [*Kroll et al.*, 2011]. In particular, the Aerodyne high-resolution aerosol mass spectrometer (HR-AMS) is a sensitive, online instrument that has been widely used in recent years for OA elemental composition measurements [*Aiken et al.*, 2008]. Recently, *Canagaratna et al.* [2015] have shown that most AMS O:C and H:C ratios published previously are underestimated due to assumptions in the data analysis that do not fully account for H_2O produced from thermally induced dehydration in the AMS and in some cases CO produced from decarboxylation. Large corrections are needed for OA that are particularly rich in specific molecular functionalities [*Canagaratna et al.*, 2015]. These corrections create uncertainties in the interpretation of previously published AMS results. In this study, we synthesize a data set of laboratory and ambient observations of the elemental ratios from surface and aircraft measurements around the world, including unpublished results. Case-by-case corrections are made according to the Improved-Ambient method described in *Canagaratna et al.* [2015]. The Van Krevelen diagram of OA composition is reevaluated in light of a decade of AMS observations and used to assess how well-reported laboratory OA represent ambient OA composition.

2. Description of Observations and Corrections

The combined HR-AMS and quadrupole AMS (Q-AMS) data set used here consists of a total of 56 surface observations at 48 locations (Figure S1 in the supporting information), in which rural/remote (21), pollution/fire-influenced (24), and downwind conditions (11) are classified. The data set has dense coverage of the Northern Hemisphere midlatitudes for both polluted and unpolluted areas. One site from the Southern Hemisphere is in the central Amazon rainforest [*Chen et al.*, 2009]. The majority of the observations are near sea level and within the boundary layer. Observations at Whistler Peak Station may sample air from the free troposphere [*Sun et al.*, 2009]. Because low $(H_2O^+)_{org}$:$(CO_2^+)_{org}$ ratios have been widely used in previous data analysis, the reported O:C and H:C ratios of OA are mostly biased low [*Canagaratna et al.*, 2015]. We apply the "Improved-Ambient" correction that uses composition-dependent factors to the surface HR-AMS data sets (see supporting information). The HR-AMS O:C and H:C ratios increase by 27 ± 7% and 11 ± 3%, respectively, on average after corrections. The Q-AMS measures the unit-mass-resolution (UMR) mass spectra of OA. Correlations of O:C and H:C with the relative intensity of UMR ions are exploited by the updated HR-AMS data and are used to estimate the corrected ratios for the Q-AMS data. The sampling information, the OA mass loadings, and both the reported and corrected O:C and H:C ratios are listed in Tables S1 and S2. Airborne HR-AMS observations are also examined in this study. The Megacity Initiative: Local and Global Research Observations (MILAGRO; C-130; 4–31 March 2006) took place in Mexico City where urban pollution and biomass burning emissions are the dominant sources of aerosol particles [*DeCarlo et al.*, 2010]. The Deep Convective Clouds and Chemistry (DC-3; DC-8; 14 May to 22 June 2012) campaign sampled air over the south central U.S. which represents a mixture of continental background air with convective outflow. The O:C and H:C ratios of OA for the airborne campaigns are reported as 1 min averages and are scaled up by 27% and 11% (the average corrections for ambient OA), respectively. The O:C and H:C ratios published previously for laboratory-generated OA are also corrected as necessary based on average corrections for similar ambient OA types (see supporting information and Table S3).

3. Results and Discussion

The Van Krevelen diagram has been used to illustrate the changes in the elemental composition of OA stemming from atmospheric processing. *Heald et al.* [2010] first showed an approximate slope of −1 for a suite of data sets including both ambient and laboratory-generated OA in this diagram. Such a slope can be produced by the simultaneous addition of both carbonyl and alcohol moieties to form a hydroxycarbonyl or carboxylic acid. A flattening of the slope at higher O:C was also observed, suggesting a tendency toward either alcohol addition or fragmentation. *Ng et al.* [2011] further examined the evolution of ambient oxygenated organic aerosol components and reported a slope of −0.5 for this subset of OA, suggesting net changes equivalent to the addition of both acid and alcohol/peroxide functional groups without fragmentation and/or the addition of acid groups with fragmentation. This study reexamines these trends for an expanded elemental ratio data set consisting of laboratory and ambient (ground and aircraft) measurements that are corrected according to recent findings.

Figure 1a shows the Van Krevelen diagram of the corrected elemental ratios for ambient OA. Campaign-average O:C and H:C ratios observed for the ground sites range from 0.3 to 0.9 and 1.3 to 1.9, respectively. OA in urban environments have the lowest O:C (ave. 0.4) and the greatest H:C ratios (ave. 1.7); O:C ratios increase (ave. 0.6) and H:C ratios decrease (ave. 1.6) for downwind locations. The remote/rural category includes forested, coastal, and agricultural locations and shows a broad range of O:C (ave. 0.7) and H:C (ave. 1.5). These O:C and H:C ratios correspond to OM:OC ratios of 1.7 for urban and 2.0 for remote/rural sites on average, which are in good agreement with the ratios of 1.6 ± 0.2 for urban and 2.1 ± 0.2 for nonurban OA derived from molecular-level measurements by *Turpin and Lim* [2001]. Airborne measurements are influenced by both surface sources and transported or chemically produced OA aloft. As shown in Figure 1a, the mean O:C and H:C ratios near surface (i.e., less than 0.5 km) for both the MILAGRO and DC-3 campaigns are similar to those for the remote/rural locations. Figure S3 shows the vertical profiles of O:C and H:C measured during MILAGRO and DC-3. The O:C increases with altitude in the mixed layer during MILAGRO, where fast photochemical aging of anthropogenic semivolatile (SVOC) and intermediate-volatility organic compounds (IVOC) can lead to highly oxidized OA [*Volkamer et al.*, 2006; *Robinson et al.*, 2007], while lower O:C at midaltitude is consistent with

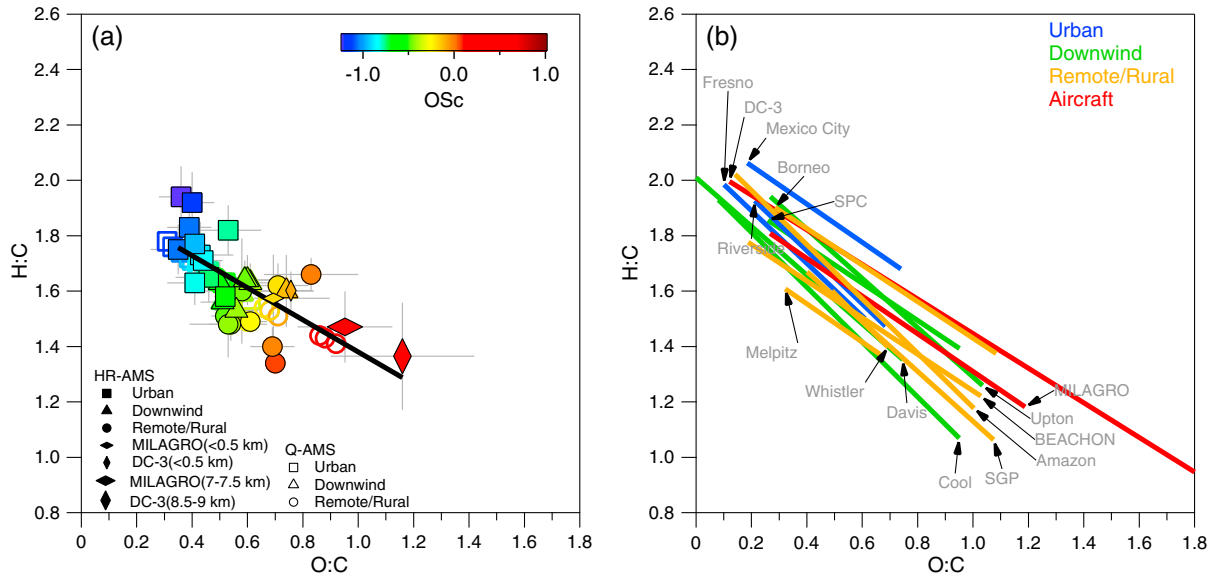

Figure 1. Van Krevelen diagrams for the O:C and H:C ratios of (a) mean surface and airborne field observations, (b) lines fitted to 15 individual campaigns from previous panel (observations with OA loadings less than 0.3 $\mu g/m^3$ are excluded). The campaign averages are shown as closed symbols for HR-AMS data and open ones (overlapped) for Q-AMS data. Error bars show the standard deviations of the observations. Black line shows the fitted line to ambient means ($R = 0.82$; Slope = -0.58 ± 0.04; Intercept = 1.96 ± 0.03). All fittings are done with the Reduced Major Axis (RMA) method.

strong influences of fresh biomass burning outflow [*DeCarlo et al.*, 2010; *Heald et al.*, 2011]. Unlike MILAGRO, the O:C increases with altitude for the DC-3 campaign, consistent with atmospheric aging. Substantial production of highly oxidized SOA in cloud or aerosol water could also increase O:C at elevated altitude, depending on the cloud type, the changes of liquid water content with altitude, and the processing time [*Lim et al.*, 2010; *Lee et al.*, 2011; *Hao et al.*, 2013]. A maximum O:C ratio of 1.16 associated with a minimum H:C ratio of 1.35 is observed for the mean values of each 0.5 km binned altitude interval, representing the most oxidized OA observed in ambient environment.

The whole data set indicates a wide range of average carbon oxidation state (OSc ≈ 2O:C–H:C) of ambient OA [*Kroll et al.*, 2011]. The OSc values range from −1.2 to +1.0 and exhibit an increasing trend from urban (ave. −0.8), downwind (−0.5), and remote/rural (−0.2) to aloft environments (+0.3). This result is consistent with the understanding of persistent oxidation during atmospheric dilution and evolution [*Jimenez et al.*, 2009]. The elemental composition of ambient OA can be fitted by a line with a slope of −0.6 and an intercept of 2.0 by the reduced-major-axis (RMA) regression method [*Smith*, 2009]. Because the Improved-Ambient correction leads to a greater percent increase in O:C than for H:C, shallower slopes are expected compared to those reported previously (e.g., −1 for bulk OA) [*Heald et al.*, 2010]. The slope and intercept for individual campaigns are different from each other (Figure 1b). The slopes range from −1.0 to −0.7 (Table S4), all steeper than the campaign mean, suggesting that the mean fit is compensating for both different slopes and different intercepts, and it is the later that flattens out the mean slope. The intercepts range from 1.8 to 2.2, and the values for urban and downwind sites (2.1–2.2) are slightly greater than the values for remote/rural sites (1.8–2.2) (Table S4). Remote regions are characterized by the largest diversity of fits. The Improved-Ambient correction of the elemental ratios increases the variability of the fits.

Figure 2 shows the bulk elemental composition of various types of laboratory-generated OA in the Van Krevelen space. The O:C and H:C ratios for fresh laboratory OA occupy a large range and tend to populate the region below and to the left of the ambient mean line (Figure 2a). Only a few measurements sit above the mean line, including fresh primary organic aerosol (POA), secondary organic aerosol (SOA) formed by isoprene photooxidation at low NO_x (i.e., HO_2 dominant conditions) [*Chen et al.*, 2011], and glyoxal uptake on particles [*Chhabra et al.*, 2010]. Lower H:C and greater O:C ratios are obtained for anthropogenic POA (APOA) and biomass burning OA (BBOA) sampled at low mass loading compared to measurements of similar systems at high mass loading, consistent with loading-dependent condensation [*Mohr et al.*, 2009;

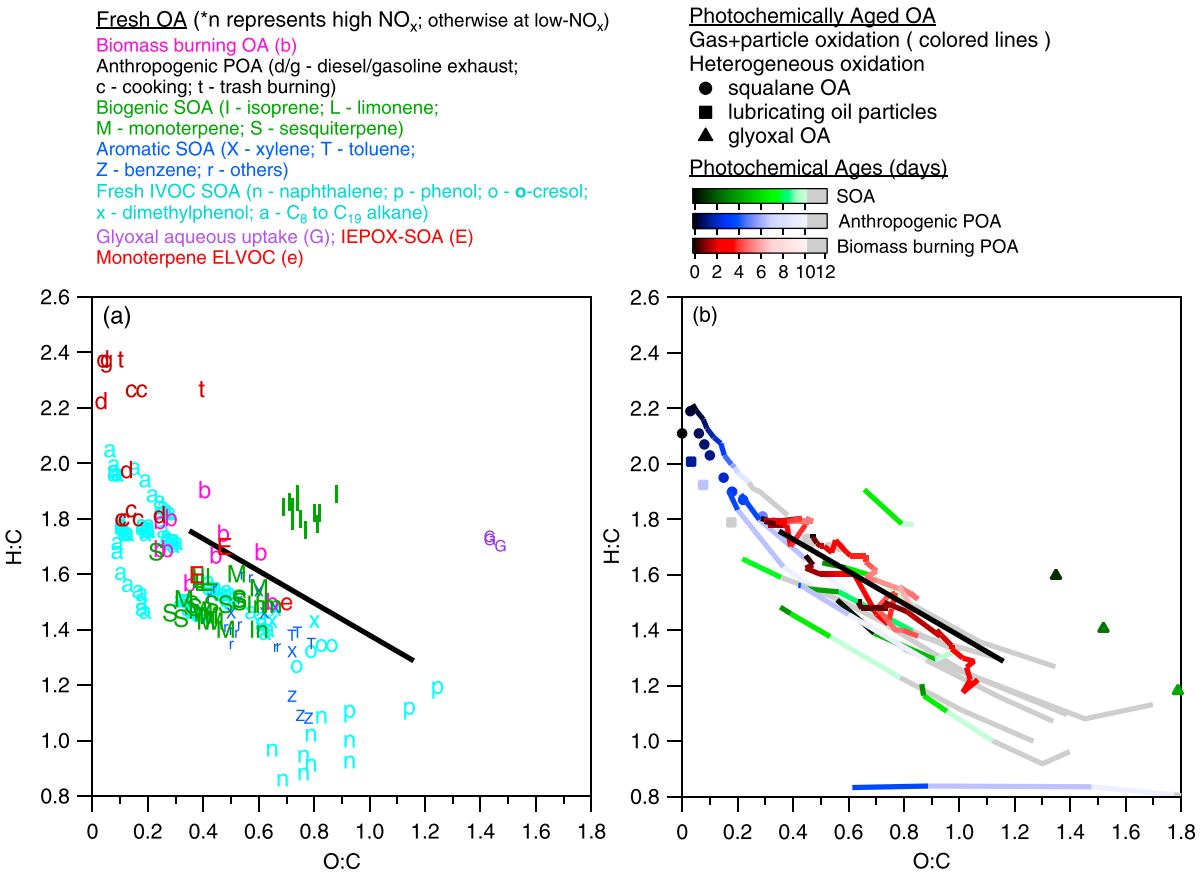

Figure 2. Van Krevelen diagrams for the O:C and H:C ratios of (a) laboratory-generated fresh OA and (b) laboratory-generated aged OA from photochemical-aging experiments. Data are taken from literature and corrected herein (Tables S1–S3). The photochemical ages are calculated based on a mean OH concentration of 1.2×10^6 molecules cm^{-3}. Black line shows the fitted line to ambient means.

Chirico et al., 2010]. The elemental ratios of fresh SOA produced by IVOC photochemical oxidation are highly dependent on carbon number and the structure of the precursors but generally lie below the ambient mean line [*Tkacik et al.*, 2012]. The compositions of POA emitted by marine sources are taken from ambient observations over regions of high oceanic biological activity and measurements of generated marine particles [*Ovadnevaite et al.*, 2011; *Frossard et al.*, 2014]. Some of the single precursor SOA data line up with a slope (e.g., −0.7 for monoterpene oxidation) [*Shilling et al.*, 2009], explained by the changes of relative abundance of SOA products that have different volatilities due to loading-dependent condensation. Reactive uptake of isoprene epoxydiol (IEPOX) forms products such as C_5-alkene triols, 2-methlytetrols, and methyltetrahydrofuran-diols that have high O:C (0.6-1) and H:C (2-2.4) [*Surratt et al.*, 2010; *Lin et al.*, 2012]. However, the bulk composition of IEPOX SOA sits below the ambient mean line with mean O:C and H:C ratios of 0.4 and 1.6 (Table S3), presumably due to other unknown products or dehydration during oligomerization [*Kuwata et al.*, 2015].

Figure 2b shows the composition changes of OA observed in laboratory photochemical-aging experiments. Similar to fresh OA, the observed elemental composition of aged OA tends to populate below the ambient mean line. The O:C ratios generally increase with higher OH exposure, and the H:C ratios decrease except for naphthalene SOA for which H:C only drops by about 10% after ~20 days of photochemical aging [*Lambe et al.*, 2011; *Ortega et al.*, 2013]. The fitted slopes for these photochemical-aging experiments range from −1.0 to −0.5, consistent with functionalization via acid addition or simultaneous acid and alcohol addition, as described above. Heterogeneous oxidation of OA leads to small increases of O:C and decreases of H:C within atmospherically relevant aging time scales (<10 days) [*Pye and Seinfeld*, 2010]. Observed slopes for squalane, lubricating oil, and glyoxal OA particles are about −1 but flat out to −0.5 when fragmentation becomes a dominant process [*Kroll et al.*, 2009; *George and Abbatt*, 2010; *Lambe et al.*, 2011].

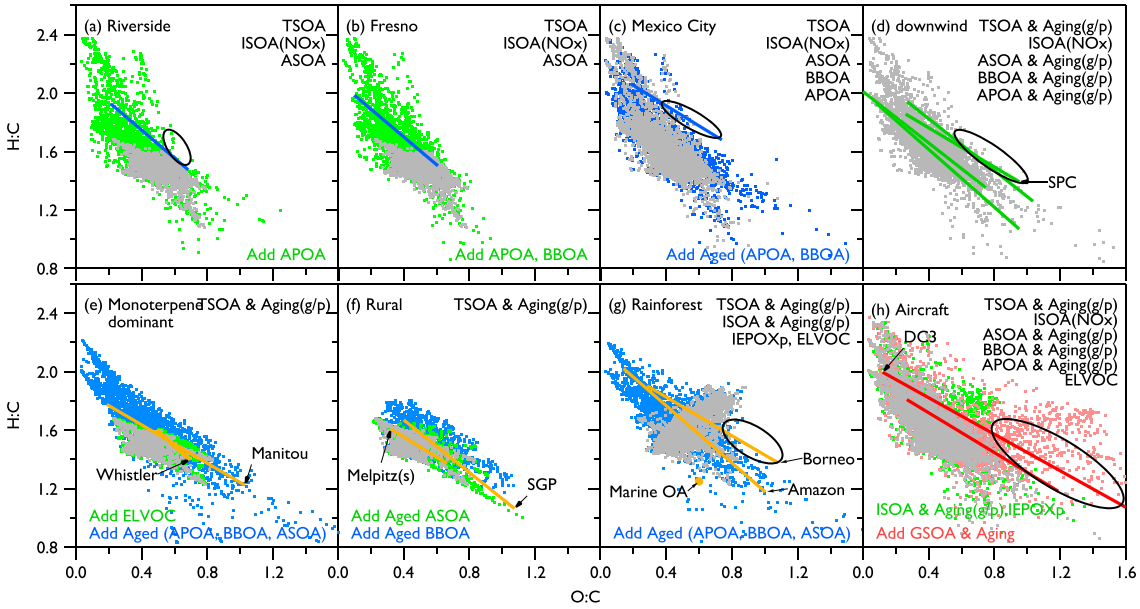

Figure 3. (a–h) Van Krevelen diagrams of simulated laboratory mixtures (dots) compared to ambient data sets (lines). Laboratory mixtures are generated randomly from classes that are indicated in the right corner of each panel. Classes include terpene SOA (TSOA), isoprene SOA produced under low (ISOA) and high NO_x (ISOA(NO_x)) conditions, aromatic SOA (ASOA), biomass burning OA (BBOA), anthropogenic POA (APOA), IEPOX SOA (IEPOXp), and extremely low volatility compounds (ELVOC) formed in monoterpene oxidation. Fitted lines to individual ambient data sets (blue: urban; green: downwind; orange: remote/rural; red: aircraft) are taken from Figure 1b. The aging data represent less than 10 days of atmospheric aging of both gas (oxidation of SVOC/IVOC and SOA) and particle-phase constituents (heterogeneous oxidation). Green, blue, and red dots represent the simulated mixtures with additional classes indicated at the bottom of the panels. Black ovals are illustrative for the space where there are dense populations of ambient data but a lack of simulated mixtures without consideration of glyoxal SOA.

Ambient OA is a complex mixture of OA from different sources and processing. Direct comparison of laboratory to ambient can be made when source contributions are known. Alternatively, statistical mixtures of laboratory OA provide a general picture of all possible compositions. The comparisons of those mixtures to ambient may reveal critical gaps regardless the uncertainties in the source apportionment. We develop a series of statistical mixtures of laboratory OA, including both diverse source types and OA obtained at different OH exposure equivalent to up to ~10 days of aging (Figure 3). For each case, we generate 5000 mixtures by combining 10 random laboratory OA compositions with uniformly distributed random mass fractions that sum up to 1. We equally weight each category of laboratory OA such that selection is not biased by the number of observations within a category.

The composition trajectories of ambient OA are generally consistent with those simulated OA mixtures, but critical gaps are revealed with this analysis. Figures 3a–3d reveal the diversity of elemental composition in polluted environments. A slope of −1.0 with an intercept of 2.1 is observed at the sites in Riverside (summer) and Fresno (winter), California (Figure 2a). During the measurement periods, fresh POA (mainly APOA) contributes about 20% of OA mass at Riverside site [*Docherty et al.*, 2011], and APOA and BBOA together contribute about 60% of OA mass at Fresno site [*Ge et al.*, 2012]. The mixtures of POA with SOA capture the majority of the ambient trajectory, suggesting that mixing rather than chemical aging dominates during the two campaigns. Another urban site at Mexico City (T0) exhibits different behavior (Figure 3c). Although fresh POA contributed nearly half of the OA mass, the observed trajectory is shallower (−0.7) with higher intercept (2.2) [*Aiken et al.*, 2009]. This shallower slope may be more consistent with chemical aging. However, the laboratory mixtures cannot capture the observations even when photochemically aged SVOC and IVOC from APOA and BBOA emissions are included. Downwind locations are characterized by composition trajectories having slopes of −0.7 to −1.0 and intercepts of 2.0 to 2.2, which extend out to higher OSc (Figure 3d) [*Saarikoski et al.*, 2012; *Setyan et al.*, 2012]. Except for San Pietro Capofiume, Po Valley site, these trajectories are captured by the statistical laboratory mixtures that further include photochemical aging of biogenic and anthropogenic SOA (gas + particle), although few points extend to the highest O:C. This is consistent with the growing importance of chemical aging moving away from source.

The observations at remote/rural locations (Figures 3e–3g) are also characterized by slopes of −0.7 to −1.0. We find that the observed trajectory at Whistler mountain during a biogenic event [*Schwartz et al.*, 2010] matches with the mixtures of fresh and aged laboratory terpene SOA (TSOA) with the addition of extremely low volatility organic compounds (ELVOC) that are produced by monoterpene ozonolysis [*Ehn et al.*, 2014] (Figure 3e). Another monoterpene-dominant site, Manitou forest, was periodically influenced by anthropogenic sources [*Ortega et al.*, 2014], and as a result, the observed trajectory agrees better with the simulated mixtures if aged pollution is included. Two other continental background sites, Melpitz (summer) and Southern Great Plains (SGP), are heavily influenced by regional secondary formation which include both biogenic and anthropogenic SOA as well as biomass burning emissions [*Martin et al.*, 2008; *Poulain et al.*, 2011]. Figure 3f shows that the observed trajectories at these two sites are reproduced by the laboratory mixtures. In particular, aged anthropogenic SOA contributes to the highest O:C population of simulated mixtures in the diagram, which are important for representing the anthropogenic influence at SGP. The Amazon and Borneo sites are highly influenced by isoprene chemistry. Figure 3g shows that the mixing of fresh and aged SOA from terpene, isoprene, ELVOC, and IEPOX could produce a +1 slope in the Van Krevelen diagram, which is completely opposite to the observations. Both sites are influenced by long-range transport of anthropogenic or biomass burning emissions as well as regional anthropogenic background [*Chen et al.*, 2009, 2014; *Robinson et al.*, 2011a, 2011b]. If we include these in the mixtures (shown as blue dots), the composition trajectory is correctly reoriented. The progression does not generally achieve the higher O:C observed in Borneo. Marine emissions may also contribute OA mass to the two sites. However, the data available for ambient marine OA falls below the trajectories and including this source would not bridge the gap [*Ovadnevaite et al.*, 2011; *Frossard et al.*, 2014].

The aircraft trajectories represent large-scale sources and transformations. Figure 3h shows that the mixtures generated from source and aged laboratory OA (grey dots) as well as IEPOX and isoprene SOA formed at HO_2-dominant conditions (green dots) capture half of the aircraft trajectories. Sources of OA having both high O:C and high H:C are missing to extend the mixtures above the ambient trajectories. Similar gaps can be found in polluted and remote tropical environments (Figures 3a, 3c, 3d, and 3g). In addition, few points extend to the highest O:C, and these mixtures must be dominated by highly aged material (~10 days). This is particularly evident for the aircraft observations (Figure 3h) but is also evident at downwind (Figure 2d), rural (Figure 3f), and forested (Figures 3e and 3g) sites. Unless the lifetime of OA in the atmosphere is greater than typically assumed, it seems unrealistic that ambient OA would be dominated by such well-aged material across this range of environments.

Aqueous-phase chemistry may be an efficient pathway across various environments to produce highly oxidized material [*Ervens et al.*, 2011, and references therein]. Water-soluble products of gas-phase photochemistry such as small carbonyls, acids, and phenolic compounds have low carbon numbers, which may produce organic acids and oligomers that have high O:C (~1-2) when reacted further with hydroxyl radicals in haze, fog, and cloud water. These products may also have high H:C (e.g., 2.0 for glycolic acid). The addition of glyoxal SOA, as an example, improves the match between laboratory and ambient aircraft data (assuming that aging is also important) (Figure 3h). However, the relative importance of aqueous-phase pathways in ambient environment remains unclear. Simulations based on the yields obtained in bulk aqueous experiments suggest substantial contribution of these pathways to the total SOA mass [*Fu et al.*, 2008; *Ervens et al.*, 2011; *Lin et al.*, 2014]. A large contribution of glyoxal SOA, however, would produce a flat slope, inconsistent with observations (Figure 3). The yields of aqueous SOA may also be lower under realistic ambient conditions. *Daumit et al.* [2014] showed that particles lose more carbon during aqueous-phase oxidation compared to in bulk solutions, causing different product distributions. The bulk elemental composition of SOA produced by aqueous oxidation from various precursors is also largely unknown and may be quite different from those of identified individual species [*Zhao et al.*, 2013]. Moreover, the relative aqueous-phase contribution to SOA depends on the time scales of gas-phase chemistry, cloud cycles, and relative humidity changes. Other possibilities for bridging the gaps include chemistry such as fast addition of alcohol or peroxide groups to APOA and BBOA, or alternatively the possibility that laboratory experiments do not adequately mimic the ambient environment. Laboratory studies typically focus on a single compound, whereas OA types and precursors are mixed in the real atmosphere [*Chen et al.*, 2011; *Tkacik et al.*, 2012; *Nakao et al.*, 2013]. Furthermore, flow-tube photochemical-aging experiments require high oxidant concentrations, which are not representative of

ambient conditions [*Lambe et al.*, 2011]. Wall losses may also lead to the underrepresentation of SOA constituents in chamber studies [*Zhang et al.*, 2014].

In summary, we show that ambient data follows a general trajectory in Van Krevelen space toward higher oxidation state. The overall fit for ambient data characterizes measurements that span a wide range of OA oxidation, providing simplifications for modeling the complex atmospheric OA system. We also show that the large diversity in the observed slope and intercept across environments can generally be explained by the generated mixtures of laboratory OA with a combination of atmospheric mixing and photochemical aging, supporting the use of laboratory measurements to explicitly constrain model framework. However, these comparisons also reveal significant gaps between ambient and laboratory measured OA composition. Sources of OA that have high O:C ($>$0.6) and, more importantly, high H:C ($>$1.6) are needed to drive the match. Aqueous-phase chemistry may be a pathway to contribute such material. Our study highlights the need to characterize the yields and bulk composition of SOA produced by aqueous-phase processing under atmospherically relevant conditions.

Acknowledgments

Data supporting Figures 1 and 2 are available as in supporting information Tables S1–S4. This work was supported by the National Science Foundation (ATM-1238109). The University of Colorado group was supported by NASA NNX12AC03G, NSF AGS-1243354, and NOAA NA13OAR4310063. Q.Z. was supported by the Office of Science (BER), DOE, DE-FG02-11ER65293. The authors thank Anne Marie Macdonald, Richard Leaitch, Andrew Lambe, Amber Ortega, Sanna Saarikoski, Niall Robinson, Yele Sun, Jesse Kroll, and other group members for helping with sampling and aspects of data analysis.

The Editor thanks two anonymous reviewers for their assistance in evaluating this paper.

References

Aiken, A. C., et al. (2008), O/C and OM/OC ratios of primary, secondary, and ambient organic aerosols with high-resolution time-of-flight aerosol mass spectrometry, *Environ. Sci. Technol.*, *42*(12), 4478–4485, doi:10.1021/es703009q.

Aiken, A. C., et al. (2009), Mexico City aerosol analysis during MILAGRO using high resolution aerosol mass spectrometry at the urban supersite (T0)—Part 1: Fine particle composition and organic source apportionment, *Atmos. Chem. Phys.*, *9*(17), 6633–6653, doi:10.5194/acp-9-6633-2009.

Canagaratna, M. R., et al. (2015), Elemental ratio measurements of organic compounds using aerosol mass spectrometry: Characterization, improved calibration, and implications, *Atmos. Chem. Phys.*, *15*(1), 253–272, doi:10.5194/acp-15-253-2015.

Chen, Q., et al. (2009), Mass spectral characterization of submicron biogenic organic particles in the Amazon Basin, *Geophys. Res. Lett.*, *36*, L20806, doi:10.1029/2009GL039880.

Chen, Q., Y. Liu, N. M. Donahue, J. E. Shilling, and S. T. Martin (2011), Particle-phase chemistry of secondary organic material: Modeled compared to measured O:C and H:C elemental ratios provide constraints, *Environ. Sci. Technol.*, *45*(11), 4763–4770, doi:10.1021/es104398s.

Chen, Q., et al. (2014), Fine-mode organic mass concentrations and sources in the Amazonian wet season (AMAZE-08), *Atmos. Chem. Phys. Discuss.*, *14*, 16,151–16,186, doi:10.5194/acpd-14-16151-2014.

Chhabra, P. S., R. C. Flagan, and J. H. Seinfeld (2010), Elemental analysis of chamber organic aerosol using an aerodyne high-resolution aerosol mass spectrometer, *Atmos. Chem. Phys.*, *10*(9), 4111–4131, doi:10.5194/acp-10-4111-2010.

Chirico, R., et al. (2010), Impact of after treatment devices on primary emissions and secondary organic aerosol formation potential from in-use diesel vehicles: Results from smog chamber experiments, *Atmos. Chem. Phys.*, *10*(23), 11,545–11,563, doi:10.5194/acp-10-11545-2010.

Daumit, K. E., A. J. Carrasquillo, J. F. Hunter, and J. H. Kroll (2014), Laboratory studies of the aqueous-phase oxidation of polyols: Submicron particles vs. bulk aqueous solution, *Atmos. Chem. Phys.*, *14*(19), 10,773–10,784, doi:10.5194/acp-14-10773-2014.

DeCarlo, P. F., et al. (2010), Investigation of the sources and processing of organic aerosol over the Central Mexican Plateau from aircraft measurements during MILAGRO, *Atmos. Chem. Phys.*, *10*(12), 5257–5280, doi:10.5194/acp-10-5257-2010.

Docherty, K. S., et al. (2011), The 2005 Study of Organic Aerosols at Riverside (SOAR-1): Instrumental intercomparisons and fine particle composition, *Atmos. Chem. Phys.*, *11*(23), 12,387–12,420, doi:10.5194/acp-11-12387-2011.

Ehn, M., et al. (2014), A large source of low-volatility secondary organic aerosol, *Nature*, *506*(7489), 476–479, doi:10.1038/nature13032.

Ervens, B., B. J. Turpin, and R. J. Weber (2011), Secondary organic aerosol formation in cloud droplets and aqueous particles (aqSOA): A review of laboratory, field and model studies, *Atmos. Chem. Phys.*, *11*(21), 11,069–11,102, doi:10.5194/acp-11-11069-2011.

Frossard, A. A., L. M. Russell, P. Massoli, T. S. Bates, and P. K. Quinn (2014), Side-by-side comparison of four techniques explains the apparent differences in the organic composition of generated and ambient marine aerosol particles, *Aerosol Sci. Technol.*, *48*(3), V–X, doi:10.1080/02786826.2013.879979.

Fu, T. M., D. J. Jacob, F. Wittrock, J. P. Burrows, M. Vrekoussis, and D. K. Henze (2008), Global budgets of atmospheric glyoxal and methylglyoxal, and implications for formation of secondary organic aerosols, *J. Geophys. Res.*, *113*, D15303, doi:10.1029/2007JD009505.

Ge, X. L., A. Setyan, Y. L. Sun, and Q. Zhang (2012), Primary and secondary organic aerosols in Fresno, California during wintertime: Results from high resolution aerosol mass spectrometry, *J. Geophys. Res.*, *117*, D19301, doi:10.1029/2012JD018026.

George, I. J., and J. P. D. Abbatt (2010), Heterogeneous oxidation of atmospheric aerosol particles by gas-phase radicals, *Nature Chem.*, *2*(9), 713–722, doi:10.1038/nchem.806.

Hao, L. Q., et al. (2013), Aerosol chemical composition in cloud events by high resolution time-of-flight aerosol mass spectrometry, *Environ. Sci. Technol.*, *47*(6), 2645–2653, doi:10.1021/es302889w.

Heald, C. L., J. H. Kroll, J. L. Jimenez, K. S. Docherty, P. F. DeCarlo, A. C. Aiken, Q. Chen, S. T. Martin, D. K. Farmer, and P. Artaxo (2010), A simplified description of the evolution of organic aerosol composition in the atmosphere, *Geophys. Res. Lett.*, *37*, L08803, doi:10.1029/2010GL042737.

Heald, C. L., et al. (2011), Exploring the vertical profile of atmospheric organic aerosol: Comparing 17 aircraft field campaigns with a global model, *Atmos. Chem. Phys.*, *11*(24), 12,673–12,696, doi:10.5194/acp-11-12673-2011.

Jimenez, J. L., et al. (2009), Evolution of organic aerosols in the atmosphere, *Science*, *326*(5959), 1525–1529, doi:10.1126/science.1180353.

Kroll, J. H., J. D. Smith, D. L. Che, S. H. Kessler, D. R. Worsnop, and K. R. Wilson (2009), Measurement of fragmentation and functionalization pathways in the heterogeneous oxidation of oxidized organic aerosol, *Phys. Chem. Chem. Phys.*, *11*(36), 8005–8014, doi:10.1039/b905289e.

Kroll, J. H., et al. (2011), Carbon oxidation state as a metric for describing the chemistry of atmospheric organic aerosol, *Nature Chem.*, *3*, 133–139, doi:10.1038/nchem.948.

Kuwata, M., S. R. Zorn, and S. T. Martin (2012), Using elemental ratios to predict the density of organic material composed of carbon, hydrogen, and oxygen, *Environ. Sci. Technol.*, *46*, 787–794, doi:10.1021/es202525q.

Kuwata, M., Y. Liu, K. A. McKinney, and S. T. Martin (2015), Physical state and acidity of inorganic sulfate can regulate the production of secondary organic material from isoprene photooxidation products, *Phys. Chem. Chem. Phys.*, *17*, 5670–5678, doi:10.1039/C4CP04942J.

Lambe, A. T., T. B. Onasch, P. Massoli, D. R. Croasdale, J. P. Wright, A. T. Ahern, L. R. Williams, D. R. Worsnop, W. H. Brune, and P. Davidovits (2011), Laboratory studies of the chemical composition and cloud condensation nuclei (CCN) activity of secondary organic aerosol (SOA) and oxidized primary organic aerosol (OPOA), *Atmos. Chem. Phys.*, *11*(17), 8913–8928, doi:10.5194/acp-11-8913-2011.

Lee, A. K. Y., P. Herckes, W. R. Leaitch, A. M. Macdonald, and J. P. D. Abbatt (2011), Aqueous OH oxidation of ambient organic aerosol and cloud water organics: Formation of highly oxidized products, *Geophys. Res. Lett.*, *38*, L11805, doi:10.1029/2011GL047439.

Lim, Y. B., Y. Tan, M. J. Perri, S. P. Seitzinger, and B. J. Turpin (2010), Aqueous chemistry and its role in secondary organic aerosol (SOA) formation, *Atmos. Chem. Phys.*, *10*(21), 10,521–10,539, doi:10.5194/acp-10-10521-2010.

Lin, G., S. Sillman, J. E. Penner, and A. Ito (2014), Global modeling of SOA: The use of different mechanisms for aqueous-phase formation, *Atmos. Chem. Phys.*, *14*(11), 5451–5475, doi:10.5194/acp-14-5451-2014.

Lin, Y. H., et al. (2012), Isoprene epoxydiols as precursors to secondary organic aerosol formation: Acid-catalyzed reactive uptake studies with authentic compounds, *Environ. Sci. Technol.*, *46*(1), 250–258, doi:10.1021/es202554c.

Martin, S. T., T. Rosenoern, Q. Chen, and D. R. Collins (2008), Phase changes of ambient particles in the Southern Great Plains of Oklahoma, *Geophys. Res. Lett.*, *35*, L22801, doi:10.1029/2008GL035650.

Mohr, C., J. A. Huffman, M. J. Cubison, A. C. Aiken, K. S. Docherty, J. R. Kimmel, I. M. Ulbrich, M. Hannigan, J. Garcia, and J. L. Jimenez (2009), Characterization of primary organic aerosol emissions from meat cooking, trash burning, and motor vehicles with high-resolution aerosol mass spectrometry and comparison with ambient and chamber observations, *Environ. Sci. Technol.*, *43*(7), 2443–2449, doi:10.1021/Es8011518.

Nakao, S., P. Tang, X. C. Tang, C. H. Clark, L. Qi, E. Seo, A. Asa-Awuku, and D. Cocker (2013), Density and elemental ratios of secondary organic aerosol: Application of a density prediction method, *Atmos. Environ.*, *68*, 273–277, doi:10.1016/j.atmosenv.2012.11.006.

Ng, N. L., M. R. Canagaratna, J. L. Jimenez, P. S. Chhabra, J. H. Seinfeld, and D. R. Worsnop (2011), Changes in organic aerosol composition with aging inferred from aerosol mass spectra, *Atmos. Chem. Phys.*, *11*(13), 6465–6474, doi:10.5194/acp-11-6465-2011.

Ortega, A. M., D. A. Day, M. J. Cubison, W. H. Brune, D. Bon, J. A. de Gouw, and J. L. Jimenez (2013), Secondary organic aerosol formation and primary organic aerosol oxidation from biomass burning smoke in a flow reactor during FLAME-3, *Atmos. Chem. Phys.*, *13*, 11,551–11,571, doi:10.5194/acp-13-11551-2013.

Ortega, J., et al. (2014), Overview of the Manitou Experimental Forest Observatory: Site description and selected science results from 2008 to 2013, *Atmos. Chem. Phys.*, *14*(12), 6345–6367, doi:10.5194/acp-14-6345-2014.

Ovadnevaite, J., C. O'Dowd, M. Dall'Osto, D. Ceburnis, D. R. Worsnop, and H. Berresheim (2011), Detecting high contributions of primary organic matter to marine aerosol: A case study, *Geophys. Res. Lett.*, *38*, L02807, doi:10.1029/2010GL046083.

Poulain, L., G. Spindler, W. Birmili, C. Plass-Dulmer, A. Wiedensohler, and H. Herrmann (2011), Seasonal and diurnal variations of particulate nitrate and organic matter at the IfT research station Melpitz, *Atmos. Chem. Phys.*, *11*(24), 12,579–12,599, doi:10.5194/acp-11-12579-2011.

Pye, H. O. T., and J. H. Seinfeld (2010), A global perspective on aerosol from low-volatility organic compounds, *Atmos. Chem. Phys.*, *10*(9), 4377–4401, doi:10.5194/acp-10-4377-2010.

Robinson, A. L., N. M. Donahue, M. K. Shrivastava, E. A. Weitkamp, A. M. Sage, A. P. Grieshop, T. E. Lane, J. R. Pierce, and S. N. Pandis (2007), Rethinking organic aerosols: Semivolatile emissions and photochemical aging, *Science*, *315*(5816), 1259–1262, doi:10.1126/science.1133061.

Robinson, N. H., et al. (2011a), Source attribution of Bornean air masses by back trajectory analysis during the OP3 project, *Atmos. Chem. Phys.*, *11*(18), 9605–9630, doi:10.5194/acp-11-9605-2011.

Robinson, N. H., et al. (2011b), Evidence for a significant proportion of secondary organic aerosol from isoprene above a maritime tropical forest, *Atmos. Chem. Phys.*, *11*(3), 1039–1050, doi:10.5194/acp-11-1039-2011.

Saarikoski, S., et al. (2012), Chemical characterization of springtime submicrometer aerosol in Po Valley, Italy, *Atmos. Chem. Phys.*, *12*(18), 8401–8421, doi:10.5194/acp-12-8401-2012.

Schwartz, R. E., et al. (2010), Biogenic oxidized organic functional groups in aerosol particles from a mountain forest site and their similarities to laboratory chamber products, *Atmos. Chem. Phys.*, *10*(11), 5075–5088, doi:10.5194/acp-10-5075-2010.

Setyan, A., et al. (2012), Characterization of submicron particles influenced by mixed biogenic and anthropogenic emissions using high-resolution aerosol mass spectrometry: Results from CARES, *Atmos. Chem. Phys.*, *12*(17), 8131–8156, doi:10.5194/acp-12-8131-2012.

Shilling, J. E., et al. (2009), Loading-dependent elemental composition of α-pinene SOA particles, *Atmos. Chem. Phys.*, *9*(3), 771–782, doi:10.5194/acp-9-771-2009.

Smith, R. J. (2009), Use and misuse of the reduced major axis for line-fitting, *Am. J. Phys. Anthropol.*, *140*(3), 476–486, doi:10.1002/ajpa.21090.

Sun, Y. L., et al. (2009), Size-resolved aerosol chemistry on Whistler Mountain, Canada with a high-resolution aerosol mass spectrometer during INTEX-B, *Atmos. Chem. Phys.*, *9*(9), 3095–3111, doi:10.5194/acp-9-3095-2009.

Surratt, J. D., A. W. H. Chan, N. C. Eddingsaas, M. N. Chan, C. L. Loza, A. J. Kwan, S. P. Hersey, R. C. Flagan, P. O. Wennberg, and J. H. Seinfeld (2010), Reactive intermediates revealed in secondary organic aerosol formation from isoprene, *Proc. Natl. Acad. Sci. U.S.A.*, *107*(15), 6640–6645, doi:10.1073/pnas.0911114107.

Tkacik, D. S., A. A. Presto, N. M. Donahue, and A. L. Robinson (2012), Secondary organic aerosol formation from intermediate-volatility organic compounds: Cyclic, linear, and branched alkanes, *Environ. Sci. Technol.*, *46*(16), 8773–8781, doi:10.1021/es301112c.

Turpin, B. J., and H. J. Lim (2001), Species contributions to PM2.5 mass concentrations: Revisiting common assumptions for estimating organic mass, *Aerosol Sci. Technol.*, *35*(1), 602–610, doi:10.1080/02786820152051454.

Volkamer, R., J. L. Jimenez, F. San Martini, K. Dzepina, Q. Zhang, D. Salcedo, L. T. Molina, D. R. Worsnop, and M. J. Molina (2006), Secondary organic aerosol formation from anthropogenic air pollution: Rapid and higher than expected, *Geophys. Res. Lett.*, *33*, L17811, doi:10.1029/2006GL026899.

Zhang, Q., et al. (2007), Ubiquity and dominance of oxygenated species in organic aerosols in anthropogenically-influenced Northern Hemisphere midlatitudes, *Geophys. Res. Lett.*, *34*, L13801, doi:10.1029/2007GL029979.

Zhang, X., C. D. Cappa, S. H. Jathar, R. C. McVay, J. J. Ensberg, M. J. Kleeman, and J. H. Seinfeld (2014), Influence of vapor wall loss in laboratory chambers on yields of secondary organic aerosol, *Proc. Natl. Acad. Sci. U.S.A.*, *111*(16), 5802–5807, doi:10.1073/pnas.1404727111.

Zhao, Y., A. G. Hallar, and L. R. Mazzoleni (2013), Atmospheric organic matter in clouds: Exact masses and molecular formula identification using ultrahigh-resolution FT-ICR mass spectrometry, *Atmos. Chem. Phys.*, *13*(24), 12,343–12,362, doi:10.5194/acp-13-12343-2013.